Electronic structure of ultrathin ordered iron oxide films grown onto Pt(111)

Th. Schedel-Niedrig,* W. Weiss, and R. Schlögl
Fritz-Haber-Institut der Max-Planck-Gesellschaft, Faradayweg 4-6, 14195 Berlin (Dahlem), Germany
(Received 17 July 1995)

It has recently been shown that well-ordered iron oxide films can be prepared epitaxially onto Pt(111) surfaces. We have investigated a one-monolayer-thick film with FeO stoichiometry and a Fe_3O_4(111) multilayer. Moreover, we prepared well-ordered multilayers with α-Fe_2O_3 stoichiometry. Core and valence level photoemission data clearly reveal that the Fe_3O_4 and α-Fe_2O_3 multilayers on Pt(111) are chemically identical to thick single crystals and polycrystalline powder samples. The x-ray-absorption near-edge structures (XANES) at the O *K* edge arise from the hybridization between O 2*p* and Fe 3*d* states as well as Fe 4*sp* states, showing that the latter also are important for the bonding interaction of the oxides. Polarization-dependent XANES measurements at the O *K* edge reveal a FeO bond length in the monolayer of 2.23±0.22 Å, which almost corresponds to the bond length in the bulk FeO (2.15 Å). The electronic structure of the iron oxides derived from the set of spectra presented will be described in terms of the ligand-field theory taking into consideration the exchange interaction between the iron 3*d* electrons.

I. INTRODUCTION

The investigation of metal-oxide single-crystal surfaces has gained increasing attention in surface science during the past years. This is because little is known about the atomic scale surface properties of these technologically important materials when compared to metals or semiconductors. The oxides of iron are used as catalyst materials,[1] and their magnetic properties are utilized for the development of high-density magnetic recording media. The preparation of clean and ordered iron oxide single-crystal surfaces is difficult. Often, these single crystals contain impurities that can segregate to the surface in ultrahigh vacuum, or they are nonstoichiometric. Furthermore, some iron oxides (FeO and Fe_2O_3) are electrical insulators, which leads to charging problems when using electron spectroscopy techniques. Their brittle nature renders difficult sample mounting and heating. One way to overcome these experimental problems is to oxidize metal single-crystal surfaces, thereby growing a thin oxide film at the surface, which has been done, for example, on single crystals of Ni and Cr.[2] Ordered Fe_3O_4 films have been prepared this way on an alloy $Ni_{60}Fe_{40}$(100) surface,[3] and different iron single-crystal surfaces were oxidized.[4] However, it is difficult to control thickness and stoichiometry of oxide films prepared this way, because the oxygen can diffuse into the substrate thereby changing these parameters. This can change the oxidation state of the surface after each thermal treatment cycle. In investigations of catalytic phenomena, the oxide surface is in contact with a very large supply of electrons from the underlying metal, which will influence the reactivity as they can interact without a metal-oxide barrier with the surface ions. Therefore, we grow thin ordered iron oxide films onto Pt(111) substrates. These epitaxial films are well defined with respect to their stoichiometries and crystallographic structures. We can control these parameters and the film thickness by choosing the proper preparation conditions, as described in Sec. II. The platinum substrate does not oxidize under the chosen preparation conditions and no oxygen diffuses into the substrate. No electrostatic charging interferes with investigations of these films by electron spectroscopy techniques or by scanning tunneling microscopy (STM).

In the present paper, x-ray and ultraviolet photoemission spectroscopy (XPS and UPS), as well as x-ray-absorption spectroscopy (XAS), have been used to characterize well-ordered films of three different iron oxides that were grown epitaxially onto Pt(111). A monolayer film with FeO stoichiometry and a Fe_3O_4 (magnetite) multilayer film have already been prepared in earlier studies.[5,7,12] Furthermore, we have prepared a multilayer film of α-Fe_2O_3 (hematite). The FeO monolayer and the Fe_3O_4 (magnetite) multilayer films grow in (111) orientation onto the substrate, whereas the α-Fe_2O_3 (hematite) multilayer film grows in (001) orientation onto the substrate, due to the common structural motif of a closed-packed arrangement of the anions, as shown in Fig. 1, and they form well-ordered structures exhibiting sharp hexagonal LEED patterns. The geometric structure of the monolayer film has been studied earlier by low-energy electron diffraction (LEED) (Ref. 5) and STM.[6] The atomic structure of the Fe_3O_4(111) surface has been determined by a dynamical LEED intensity analysis, using the Tensor LEED technique.[7] The valence-band and core-level photoemission experiments on the 10-ML-thick Fe_3O_4 and α-Fe_2O_3 films mostly agree with earlier studies performed on polycrystalline samples[1,8] and on diamond scraped,[9] as well as on cleaved single-crystal surfaces.[10] Our XAS measurements on these films also are in line with earlier studies performed on polycrystalline samples.[11] This further indicates the chemical and structural identity of the epitaxial films with bulk material and demonstrates that it is

0163-1829/95/52(24)/17449(12)/$06.00

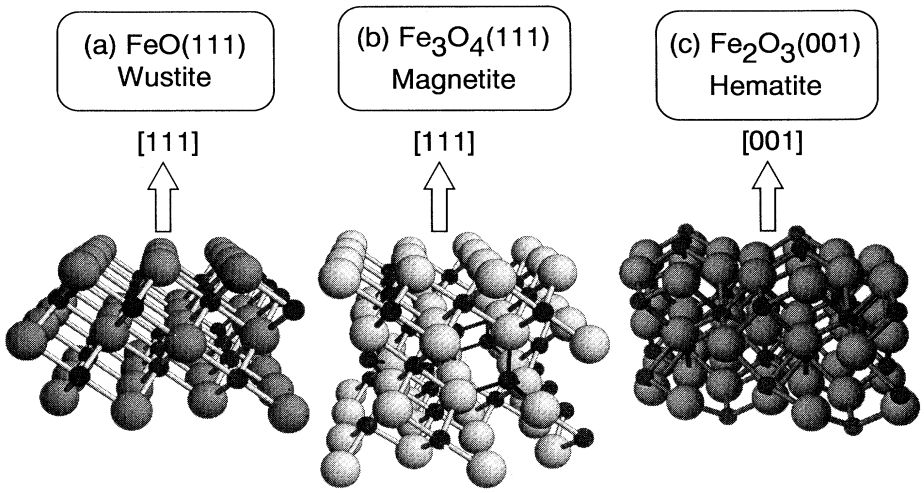

FIG. 1. Perspective side views of ideal bulk terminated iron oxide surfaces: (a) FeO(111) wustite, (b) Fe_3O_4(111) magnetite, and (c) α-Fe_2O_3(001) hematite. FeO (wustite) crystallizes in the cubic sodium chloride structure and contains Fe^{2+} cations (indicated by small filled circles) octahedrally coordinated to the oxygen anions. Fe_3O_4 (magnetite) is ferromagnetic and has a cubic inverse spinel structure with Fe^{2+} cations in octahedral sites and Fe^{3+} cations in both octahedral and tetrahedral sites, the latter indicated by solid bonds. α-Fe_2O_3 (hematite) is antiferromagnetic and has the hexagonal crystal structure of corundum with Fe^{3+} cations located in a slightly distorted oxygen environment.

possible to prepare them in a controlled way onto platinum substrates. The polarization-dependent XAS measurements on the monolayer film indicate that Fe^{2+} ions are coordinated trigonally by O^{2-} ions and that the iron-oxygen bond length in the monolayer is in good agreement with the bond length in the FeO bulk structure. This supports the structure model proposed for this film in Ref. 5, which postulates that the film consists of an iron-oxygen bilayer with iron atoms forming the first layer on top of the platinum substrate.

In Sec. II, the experimental instrumentation and the preparation of the platinum substrate as well as the iron oxide films are described. The photoemission spectroscopy data are presented and discussed in Sec. III (core-level XPS) and Sec. IV (valence-band UPS). In Sec. V, the XAS measurement will be presented and then discussed in Sec. VI.

II. EXPERIMENT

A. Instrumentation

All experiments were performed in a vacuum generator double-chamber ultrahigh vacuum (UHV) system with a base pressure of less than 1×10^{-10} mbar, which was attached to the SX700-I beamline at the Berliner Synchrotron Radiation source BESSY. An extra reaction chamber was equipped with an iron evaporation source and an oxygen resistant sample heating station. This chamber can be filled with gases up to pressures of 1000 mbar, which allows controlled oxidation of metal films far away from UHV conditions up to temperatures of about 1500 K. The analysis chamber was equipped with an Omicron backview LEED optic and a Vacuum Generator CLAM electron energy analyzer. The source for the XPS measurements was a unmonochromatized Mg $K\alpha$ line ($h\nu=1253.6$ eV), with an estimated instrumental broadening of 0.9 eV. The photon-energy-dependent UPS measurements and the XAS measurements were performed with the monochromatized synchrotron radiation at the SX700 I beamline, which provides photon energies from 10 to 2000 eV. The monochromator was operated with a resolution of 0.2 at 150 eV photon energy, 1.3 eV at the O K edge and 2.0 eV at the Fe $L_{2,3}$ edge. The photon energy was calibrated to an accuracy of ±0.5 eV, by reference to the La $3d\rightarrow4f$ transition at 836 eV of a $LaAl_2$ sample. The electron energy analyzer is used for the photoemission experiments and a partial-electron-yield detector equipped with two commercial multichannel plates *(Hamamatsu)* for the XAS measurements. All XAS data were collected in the partial-electron yield modus (-450 V retarding voltage), in order to increase the surface sensitivity leading to a probing depth comparable to XPS. The partial yield is proportional to the absorption coefficient, provided that the mean free path of the collected electrons is small compared to the absorption length. To avoid possible problems with the spectral artifacts to oxygen and iron contaminations of optical components, the spectra were divided by the spectrum from a clean Pt(111) surface recorded under the same conditions and were subsequently normalized to the edge jumps. The valence-band photoemission energy distribution curves (EDC's) from each of the iron oxide samples are referenced to the Fermi level, as determined from the clean Pt(111) substrate.

B. Preparation of the substrate and of the iron oxide films

All preparations were performed in the reaction chamber described above. The platinum single crystal

could be heated resistively with currents up to 60 A. Its temperature was measured with a Chromel-Alumel thermocouple that could be moved onto the surface during the annealing procedure by a linear feedthrough. The Pt(111) surface was prepared by repeated cycles of 1-keV Ar^+-ion bombardment in the second UHV chamber and subsequent annealing to $T=1500$ K in 2×10^{-7} mbar O_2 in the reaction chamber. A final flash to 1500 K without oxygen resulted in a clean surface, as confirmed by XPS and in a sharp hexagonal (1×1) LEED pattern. Onto this clean Pt(111) surface a 1-ML-thick iron oxide film with FeO stoichiometry and 10-ML-thick Fe_3O_4 films were prepared as described earlier.[7] In this work, we determined the overlayer thickness by measuring the intensity attenuation of the substrate Pt $4f$ core-level signal, considering the mean free path of the electrons. Because of the lattice mismatch the FeO monolayer forms a coincidence structure on the platinum substrate that creates a sharp hexagonal LEED pattern, where each main spot is surrounded by six satellite spots, as described in detail in Ref. 5. Presumably this film consists of an iron-oxygen bilayer with the iron lying on top of the platinum substrate surface. This coincidence structure also has been imaged directly by scanning tunneling microscopy.[6] Well-ordered 10-ML-thick Fe_3O_4 films exhibiting a sharp hexagonal (2×2) LEED pattern were obtained after several cycles of iron deposition and subsequent oxidation in 10^{-6} mbar oxygen at $T=1000$ K. The (2×2) superperiodicity in this LEED pattern arises from the iron cation positions in between the close-packed oxygen (111) planes of the Fe_3O_4 magnetite structure. They form a (2×2) supercell, with respect to a (1×1) cell on these oxygen layers. The iron cations in the hexagonal corundum structure of α-Fe_2O_3 hematite form a $(\sqrt{3}\times\sqrt{3})R30°$ supercell with respect to the (1×1) cell in the close-packed oxygen (001) layers.[12] In a second preparation cycle, the 10-ML-thick magnetite film has been oxidized for 5 min at $T=1000$ K under 30-mbar oxygen partial pressure. This produced a well ordered and clean α-Fe_2O_3 film that exhibited a sharp hexagonal $(\sqrt{3}\times\sqrt{3})R30°$ LEED pattern. The hematite film was stable in ultrahigh vacuum and could be studied after its preparation by all the techniques described above.

III. XPS MEASUREMENTS

The Fe $2p$ and O $1s$ core-level spectra of the different iron oxide films prepared onto Pt(111) are shown in Fig. 2. Traces (a) show the Fe_xO(111) monolayer, (b) the 10-ML-thick Fe_3O_4(111) magnetite film, and (c) the 10-ML-thick α-Fe_2O_3(001) hematite film. The iron $2p$ core levels are split into $2p_{1/2}$ and $2p_{3/2}$ components, due to the spin-orbit coupling. The Fe $2p_{3/2}$ core levels of the α-Fe_2O_3(001) multilayer film and of the FeO(111) monolayer film appear at 711.3 eV and 710-eV binding energy, respectively. These values are characteristic for the Fe^{3+} and Fe^{2+} species and agree well with literature data.[1,8] Additionally, on α-Fe_2O_3, we observe a shake-up satellite line characteristic for the Fe^{3+} species[8] at 719.2-eV binding energy as indicated in Fig. 2. The Fe $2p_{3/2}$ signal in the Fe_xO(111) monolayer spectrum is slightly broadened when compared to the α-Fe_2O_3 spectrum and shows an asymmetric high binding-energy side that can be attributed to a satellite excitation of the Fe^{2+} species.[1] Magnetite Fe_3O_4 contains two-third Fe^{3+} ions and one-third Fe^{2+} ions, leading to broader Fe $2p$ signals in the XPS spectrum, as compared to the Fe $2p$ core-level lines of the α-Fe_2O_3(001) multilayer. The O $1s$ spectra of all iron oxides are located at 530.1-eV binding energy. This agrees well with the literature,[1,8] as it is known that the O $1s$ binding energy is independent of the iron oxide phase. In the spectra from multilayers of Fe_3O_4(111) and α-Fe_2O_3(001) a broad satellite excitation can be observed centered at about 537.3 eV, which should have the same physical origin as the Fe^{3+} satellite signal observed on the hematite α-Fe_2O_3 film. The spectrum [Fig. 2(a)] from the monolayer shows an increasing background intensity towards lower binding energies, which is due to the substrate Pt $4p_{3/2}$ core level located at 519.4 eV binding energy.

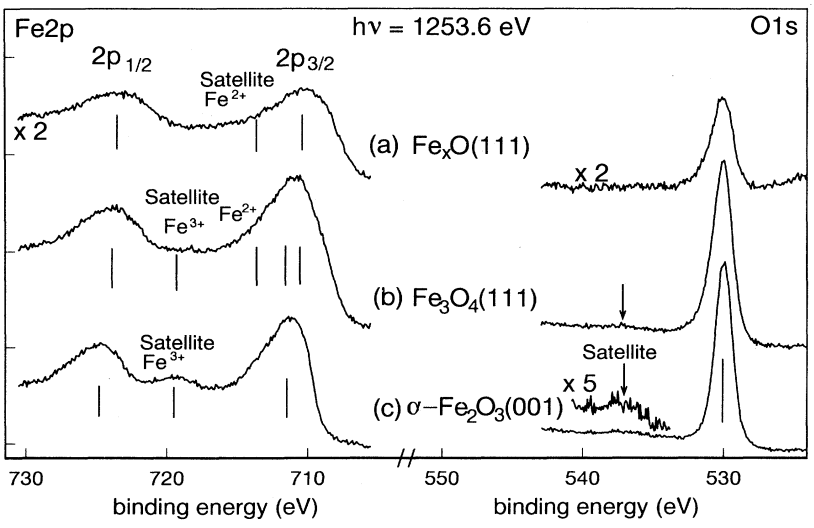

FIG. 2 O $1s$ and Fe $2p$ core-level photoemission spectra of ordered iron oxide films grown onto Pt(111) taken at $h\nu=1253.6$ eV: (a) 1-ML-thick film with Fe_xO stoichiometry, (b) 10-ML-thick Fe_3O_4(111), and (c) 10-ML-thick α-Fe_2O_3(001) film.

IV. VALENCE-BAND PHOTOEMISSION

The valence bands from the iron oxides are made up of Fe $3d$ states that are hybridized with O $2p$ states. This hybridization and the complexity of electron correlation effects make the interpretation of the valence-band photoemission spectra difficult. Early studies on Fe_xO single-crystal surfaces revealed the dominance of Fe $3d$ state emission features relative to O $2p$ states at high proton electron energies.[13] The analysis was based on localized Fe $3d$ states in a ligand field of the oxygen anions and the spectra were interpreted with the help of calculated crystal-field split final states. Another study showed the Fe $3d$ valence-band features to extend 10 eV below the Fermi energy.[8]

Synchrotron radiation allows us to measure the resonant photoemission effects of Fe $3d$ derived states when the photon energy is tuned near the Fe $3p$ excitation threshold in iron oxides. This was done for the first time by Fujimori *et al.* on *in situ* scraped surfaces of Fe_xO and α-Fe_2O_3 single crystals.[9] These experiments have shown that excitations of the type $3p^6 3d^n \rightarrow [3p^5 3d^{n+1}]^*$ (the asterisk denotes an excited state) dominate at the $3p$ threshold and that these excitations decay to a $3p^6 3d^{n-1} + e^-$ state thereby resonantly enhancing the direct photoemission process $3p^6 3d^n \rightarrow 3p^6 3d^{n-1} + e^-$. By taking the difference between valence-band EDC's measured just above and below the Fe $3p \rightarrow 3d$ resonance energy, the nonresonating O $2p$ contributions were eliminated and the distribution of Fe $3d$ derived final states is obtained. It consists either of pure Fe $3d$ states or of Fe $3d$-derived states that are hybridized with neighboring oxygen ligands. Furthermore, constant-initial-state spectra measured across the Fe $3p$ excitation threshold can be used to distinguish the $3d^{n-1}$ from the $3d^nL$ photoemission final states, i.e., one can identify hybridized Fe-O states in the valence band (L is a hole state in the oxygen ligand).[9,14] These studies revealed that in all the different iron oxides, $3d^nL$ final states are located predominantly between the Fermi level and 9-eV binding energy, whereas $3d^{n-1}$ final states are located between 9- and 16-eV binding energy. These observations and the large spectral valence-band width of 16 eV can be modeled by configuration-interaction cluster calculations on $[FeO_6]^{10-}$ and $[FeO_6]^{9-}$ clusters, representing FeO and α-Fe_2O_3.[9]

In Fig. 3, the angle-integrated valence-band EDC's are shown (a) of a 10-ML-thick Fe_3O_4 film taken with $h\nu = 120$ eV photon energy and (b) of a 10-ML-thick α-Fe_2O_3 film taken with $h\nu = 100$ eV photon energy. In the Fe_3O_4 spectrum, a feature at 1.2-eV binding energy can be seen, which is not present in the α-Fe_2O_3 spectrum. This state is assigned to a $3d^6L$ final state of Fe^{2+} ions in the Fe_3O_4 film. In both spectra, the main intensity arises from Fe $3d$ states, which are concentrated between 2- and 8-eV binding energy. This follows from the atomic cross-section ratio, which is weighted by the number of electrons per (isolated) atom, $\sigma(\text{O } 2p)/\sigma(\text{Fe } 3d) \cong 0.1$ for 100-eV-photon-energy excitation.[36] We also see $3d^4$ final-state emission between 10- and 18-eV binding energy

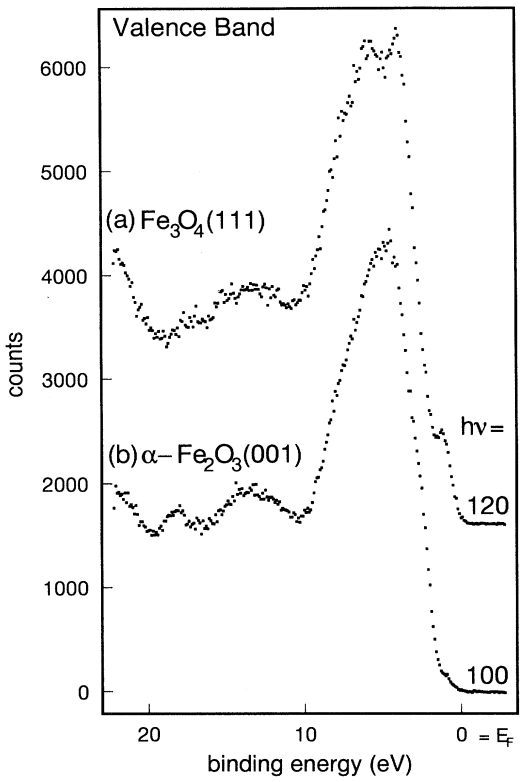

FIG. 3. Valence-band photoemission spectra of (a) 10-ML-thick Fe_3O_4(111) and (b) 10-ML-thick α-Fe_2O_3(001) films.

in the α-Fe_2O_3 film, whereas in the Fe_3O_4 film containing Fe^{2+} and Fe^{3+} ions, these features are less pronounced, due to overlapping $3d^4$ and $3d^5$ final states. In addition to the LEED patterns observed on these two films, the photoemission measurements also indicate that we prepared single phased Fe_3O_4 magnetite and α-Fe_2O_3 hematite films onto the Pt(111) substrate.

The angle-integrated valence-band EDC's of the Fe_xO(111) monolayer are shown in Fig. 4. The spectra are taken just above [$h\nu = 60$ eV, Fig. 4(a)] and below [$h\nu = 50$ eV, Fig. 4(b)] the Fe $3p$ threshold. The corresponding spectra of a cleaved Fe_xO(100) single-crystal surface measured by Lad and Henrich[10] are shown below each spectrum for comparison. Significant changes are visible in the shape of the valence-band spectra, as the $3d$ states resonate above the $3p$ excitation threshold ($h\nu = 60$ eV). The difference spectrum between spectra (a) and (b) reflecting the Fe $3d$ derived final states is shown at the bottom. The $3d$-derived states extend 20 eV below the Fermi level, which is in general agreement with the results of Lad and Henrich for a cleaved Fe_xO(100) single-crystal surface, as shown at the bottom of Fig. 4. However, the region between the Fermi level and 10 eV below exhibits a different overall shape for the Fe_xO(111) monolayer when compared to the single-crystal spectrum. This suggests that iron-platinum bonds were formed at the substrate-overlayer interface leading to Fe $3d$ final-state features coupled with the platinum electronic states.

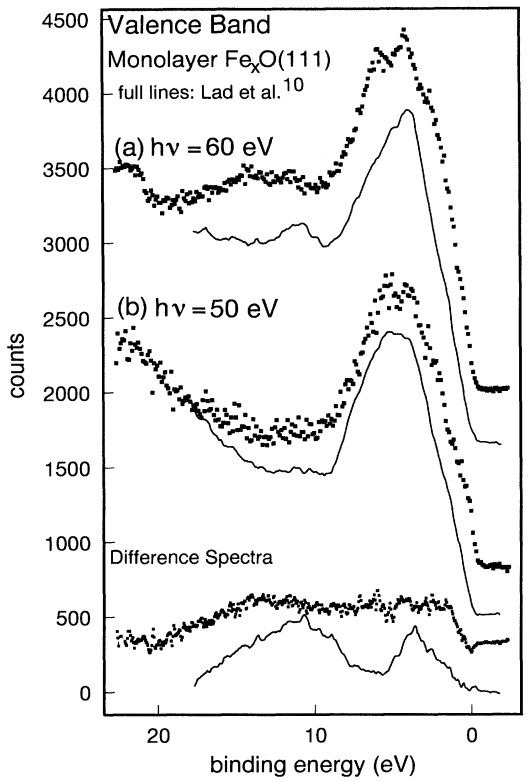

FIG. 4. Valence-band photoemission spectra of a 1-ML-thick iron oxide film with Fe_xO stoichiometry. The valence band is taken (a) with $h\nu=60$ eV photon energy above and (b) with $h\nu=50$ eV photon energy below the Fe $2p$ edge (at 55 eV). Also shown are the corresponding valence-band data performed on cleaved FeO(100) single-crystal surfaces (full lines below each spectrum, Ref. 10) for comparison. At the bottom, the difference spectrum reflecting the Fe $3d$ final states is given and compared with the difference spectrum taken from Ref. 10.

V. X-RAY-ABSORPTION NEAR-EDGE SPECTROSCOPY (XANES)

The oxygen K- and transition-metal (TM) $L_{2,3}$-edge absorption spectra of oxides can be readily measured using synchrotron radiation, not in a conventional absorption geometry, but rather using the electron yield technique. X-ray absorption (XAS) is a local process in which a core-level electron is promoted to an excited electronic state, which can be coupled to the original core level by the dipole selection rule. For the oxygen K edge ($L=0$), this means that only oxygen p character states ($L=1$) can be reached. The resulting spectrum can be interpreted in a first-order approximation as an image of the oxygen p projected unoccupied density of states (DOS). A fundamental problem arises in relating a calculated DOS to an XAS spectrum, due to the interaction of the excited electron in the final state with its surrounding. This modifies the apparent DOS because of correlation effects. Moreover, the created core hole affects the final-state DOS, as has been shown for the early-transition-meal $2p$ ($L_{2,3}$) XAS spectra.[11] For the oxygen K edges, these effects probability are less severe compared to the transition-metal $L_{2,3}$ edges, because the core hole is located at the oxygen site, while the states in the unoccupied bands just above the Fermi level exhibit their spectral weight mainly on the metal sites. Oxygen $2p$ orbitals hybridize with these unoccupied metal bands which are, however, only indirectly affected by a O $1s$ core hole.

The method is not only a probe of unoccupied valence-band states, but also a useful tool for determining molecular orientations.[16,17] This is due to the polarization dependence of the various resonances, i.e., the variation of their intensity as a function of the orientation of the **E** vector of the light relative to some symmetry elements of the structure.[18] Since XAS is a local process in which an electron is promoted to an excited electronic state, the determination of the TM-to-oxygen bond directions should be possible, provided that the O $2p$ final states are hybridized with metal d states. In a simple model, the transitions at the O K edge can be grouped into two types: antibonding $pd\pi$ resonances, which are polarized perpendicular to the TM-oxygen bonds and antibonding $pd\sigma$ resonances, which are polarized along the TM-oxygen bonds.

A. Oxygen K edge

Figure 5 shows the O K-edge absorption spectra of the ordered iron oxide films grown onto the Pt(111) surface for two angles Θ_e between the **E** vector of the light and the surface normal, $\Theta_e=20°$ and 90°. In the upper right-hand side of Fig. 5, the hexagonal (1×1) LEED pattern is indicated schematically with the surface lattice unit vectors in reciprocal space (**a*** and **b***) and real space (**a** and **b**). All spectra are detected along the azimuthal direction of the real-space unit vector **a**. (a) shows the $Fe_xO(111)$ monolayer, (b) the $Fe_3O_4(111)$ multilayer, and (c) the α-$Fe_2O_3(001)$ multilayer. The bold arrows mark the Fermi-level positions, as determined from the O $1s$ core-level spectra (see Fig. 2). The intensities of the XAS spectra were normalized to the edge jump at ~555-eV photon energy. The spectra exhibit strong structures up to 20 eV above the threshold. Oxygen K-edge data of thin epitaxial ordered iron oxide films are presented here for the first time. The data for α-Fe_2O_3 and Fe_3O_4 are in good agreement with the high-resolution data that exist for natural mineral samples of α-Fe_2O_3 and Fe_3O_4.[19] There is also a general agreement with electron-energy-loss spectroscopy (EELS) data for Fe_xO, Fe_2O_3, and Fe_3O_4 thin films.[20]

One can divide the spectra in Fig. 5 to two regions: the first region directly at the threshold is assigned to oxygen $2p$ weight in the states of mainly transition-metal $3d$ character: the transition-metal $3d$ band. This assignment agrees with molecular-orbital calculations.[21,22] The second region, typically 5–20 eV above the threshold, is attributed to oxygen $2p$ states hybridized with metal $4s$ and $4p$ states.[19,23] The large spread in energy for the oxygen $2p$ character is an indication of significant covalency in these oxides. In Fig. 5, a common structure of the $4sp$ band at ~542-eV photon energy is observed for all iron

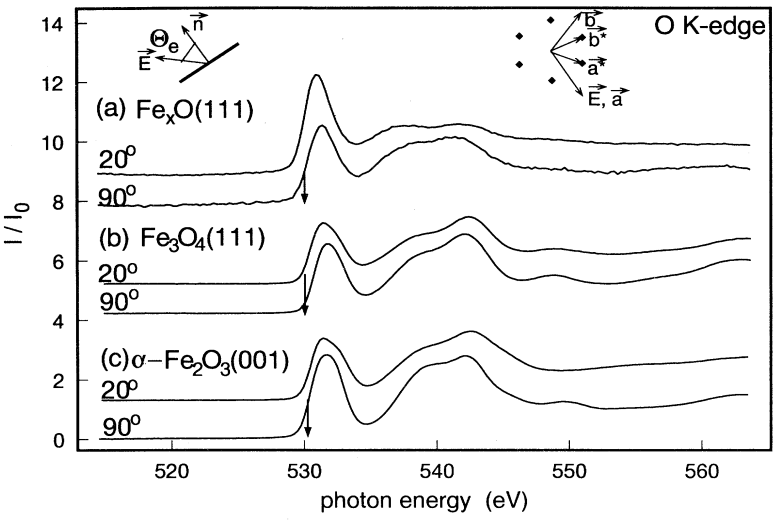

FIG. 5. The O K-edge x-ray-absorption spectra of ordered iron oxide films on Pt(111): (a) 1-ML-thick film with Fe_xO stoichiometry, (b) 10-ML-thick Fe_3O_4(111), and (c) 10-ML-thick α-Fe_2O_3(111) film. All spectra are shown for two angles between the **E** vector of the light and the surface normal, $\Theta_e = 20°$ and 90°. The arrows indicate the XPS core-level positions, as shown in Fig. 2. At the upper right the schematic (1×1) LEED pattern with the surface lattice real space (**a** and **b**) and reciprocal space (**a*** and **b***) unit vectors is shown.

oxide films prepared in this work. It consists of a double peak separated by ~3.8 eV for the multilayers and ~4.5 eV for the monolayer film. In accordance to the O K edges of the 3d-TM oxides,[19] this structure can be related to the symmetry set up by the nearest oxygen neighbors. In Fe_2O_3, oxygen ions octahedrally surround the Fe^{3+} ions and in Fe_3O_4, oxygen ions octahedrally and tetrahedrally surround the Fe^{3+} and Fe^{2+} ions. The increased splitting of ~4.5 eV for the Fe_xO(111) monolayer indicates a different local surrounding of the Fe^{2+} cations in the monolayer film.

We observed a different intensity ratio between the first sharp unoccupied band arising from O 2p Fe 3d hybrid states at ~531 eV and the broader O 2p Fe 4sp derived hybrid bands at ~542 eV: for the spectrum from the Fe_xO(111) monolayer [Fig. 5(a)], the intensity of the O 2p Fe 3d derived bands is increased relative to the O 2p Fe 4sp bands, whereas this intensity ratio is decreased in the multilayer spectra of Fe_2O_3 and Fe_3O_4. The reason for this may be the increase in the number of unoccupied 3d states *available* for mixing with O 2p states (hybridization) within the monolayer, which can be related to either the different local surroundings of the iron cations within the mono- and multilayers or to the coupling of occupied Fe 3d states with unoccupied Pt 5d states at the substrate-overlayer interface. Additionally, there is a variation in intensity for the monolayer as Θ_e is varied, pointing towards a polarization dependence of the O 1s→O 2p Fe 3d/O 2p Fe 4sp transitions. They exhibit a maximum/minimum at high angles of light incidence, $\Theta_e = 20°$. We can exclude this polarization dependence to be caused by shadowing effects that may occur on very rough surfaces or by the coexistence of differently oriented crystallites or even larger polycrystalline parts in these films. This is concluded from the LEED patterns of both the monolayer and multilayer films that exhibit sharp spots and low background intensities. No extra spots from misoriented crystallites as well as no spot splitting or extreme spot broadening, due to high surface step densities is observed.[5] The STM images of the monolayer films always show smooth and flat surfaces with monatomic steps that are one Pt(111) layer distance high.[6]

This indicates that we were able to detect iron-oxygen bond directions within the monatomic film. In contrast to the monolayer, the O 2p Fe 3d/O 2p Fe 4sp derived bands in the multilayer spectra only show small intensity variations as a function of the E-vector polarization direction. An averaging of the intensity variation occurs, due to the isotropic bonding of iron in the voids of a three-dimensional closed-packed lattice.

B. Iron $L_{2,3}$ edges

The Fe $L_{2,3}$ edges of the different iron oxide films on Pt(111) are shown in Fig. 6 for two angles between the **E** vector of the light and the surface normal, $\Theta_e = 20°$ and 90°, detected along the indicated azimuthal direction **a**. Trace (a) belongs to the Fe_xO(111) monolayer, (b) to the Fe_3O_4(111) multilayer, and (c) to the α-Fe_2O_3(001) multilayer. The difference spectra (20°–90°) are also shown. The bold arrows mark the Fermi-level positions, as determined from the Fe 2p core-level spectra shown in Fig. 2. All spectra in Fig. 6 were normalized to the edge jump at ~735-eV photon energy. They exhibit rather similar profiles with two white lines labeled L_3 and L_2, which are separated to a first approximation by the spin-orbit splitting of the Fe $2p_{3/2}$ and Fe $2p_{1/2}$ core levels.

High-resolution XAS data on the Fe $L_{2,3}$ edges lines for α-Fe_2O_3 and Fe_3O_4 have recently been published[24] and show a splitting of the white lines, which is not observed in the present data, due to the reduced energy resolution of 2.0 eV. On the other hand, the $L_{2,3}$ edge in the iron oxides has been a favorite feature for EELS studies, since the first notice of the anomalous L_3/L_2 white-line ratio in the iron metal.[25] A more complete work has compared several spectral properties between iron metal and the FeO phase.[26] There is a chemical shift of 1.4 eV, a reduction of the white-line width from 3.5 to 2.4 eV in the oxide, and the increase of the intensity ratio $I(L_3)/I(L_2)$ from 3.0 to 4.1 (or from 3.4 to 5.5, depend-

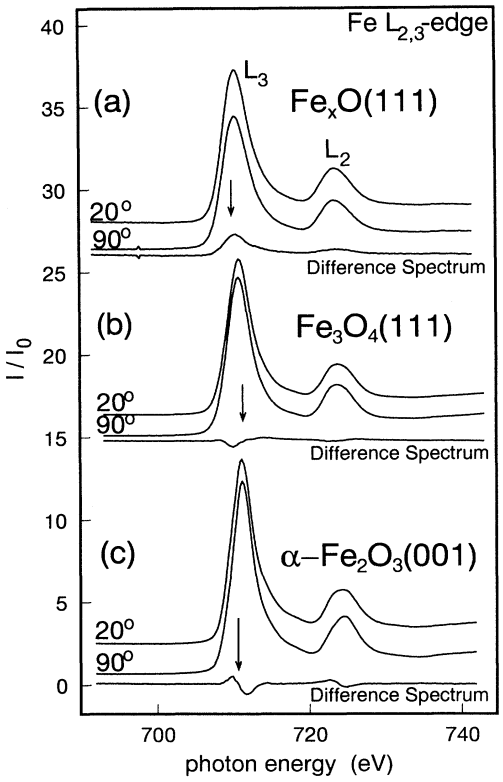

FIG. 6. The corresponding Fe $L_{2,3}$-edge x-ray-absorption spectra of the ordered iron oxide films: (a) 1-ML-thick film with Fe_xO stoichiometry, (b) 10-ML-thick $Fe_3O_4(111)$, and (c) 10-ML-thick α-$Fe_2O_3(001)$ film. All spectra are shown for two angles between the **E** vector of the light and the surface normal, $\Theta_e = 20°$ and 90°. The arrows indicate the XPS core-level position, as shown in Fig. 2. Also shown are the difference spectra (20°–90°) below each pair of spectra.

ing on the method used for the integration of the white line). Several studies have extended this approach to different oxides: the chemical shift has been attributed to valence change ($Fe^{2+} \rightarrow Fe^{3+}$) and to coordination modification (octahedral → tetrahedral) in various complex iron compounds.[27] A confirmation of the regular variation in the $I(L_3)/I(L_2)$ ratio through the *d*-transition series is given in Ref. 15. A high-resolution EELS study on the three oxide phases reveals extra fine structures on the white lines[28] and the splittings of the white lines have been assigned to the oxidation state and coordination number for iron in four model minerals.[29] It has very recently been postulated that the white lines are due to $2p^6 3d^n \rightarrow 2p^5 3d^{n+1}$ transitions, and that the recorded changes of relative intensity—$I(L_3)/I(L_2)+I(L_3)$ (or branching ratio)—are mainly governed by strong Coulomb and exchange interactions on the excited atom.[30] Furthermore, the spectra have been simulated by calculating the projection of the atomic multiplets in octahedral symmetry.[31]

One can observe intensity variations of the two white lines at ~711 and ~724 eV as Θ_e is varied. The difference spectrum for the Fe_xO monolayer shows that there is a variation in intensity of about 16%—with respect to the white line at the L_3 edge taken at $\Theta_e = 90°$. The Fe $2p \rightarrow$Fe $3d$ derived transitions are polarization dependent, and the white lines exhibit a maximum at high angles of incidence, $\Theta_e = 20°$. This intensity variation is nearly identical with the intensity variation of the O $2p$ Fe $3d$-derived band at ~531 eV at the O K edge [see Fig. 5(a)], where a variation of 25% is found, suggesting that the observed polarization dependence at the two edges have the same physical origin. The features of the multilayer spectra exhibit, on the other hand, only a small polarization dependence.

It is important to note that the difference spectrum of the α-$Fe_2O_3(001)$ multilayer shown at the bottom of Fig. 6(c) exhibits the same polarization dependence as the one caused by linear magnetic dichroism, which was observed very recently at the Fe $L_{2,3}$ edge of a single crystalline antiferromagnetic α-Fe_2O_3 (hematite) sample.[32] The α-Fe_2O_3 crystal has been found to be a model system, which provides clear evidence for magnetic linear dichroism in an antiferromagnet and the magnetic origin of this dichroism has been demonstrated by the Morin transition at $\approx -10\,°C$, where the moments in α-Fe_2O_3 rotate by 90°. At 300 K, the magnetic moments are aligned perpendicular to the trigonal **c** axis of the α-Fe_2O_3 single crystal forming three 120° domains, and at low temperatures the moments are rotated by 90° and, therefore, are aligned parallel to the **c** axis. Since we change the orientation of the **E** vector of the light relative to the **c** axis [which corresponds to the [001] direction of the hexagonal unit cell of hematite, see Fig. 1(c)] by rotating the sample from normal light incidence, where **E** is aligned perpendicular to **c**, to the grazing light incidence where **E** nearly is parallel to the **c** axis, the observed features in the difference spectrum shown at the bottom in Fig. 6(c) presumably have their origin in the x-ray linear magnetic dichroism of the hematite film. This further indicates that we prepared a single phased α-Fe_2O_3 film onto the Pt(111) substrate.

VI. DISCUSSION

In a pure ionic model, the oxide anion would have the configuration O $1s^2 2s^2 2p^6$ and the $1s \rightarrow 2p$ channel would be closed in XAS. Covalence reduces the number of filled states with O $2p$ character, so that the strength of the O $1s$ signal at the threshold is related to the degree of covalency. It is well known that the transition-metal oxides are not composed of pure ions, but exhibit a considerable covalent contribution to their bonding and that the oxygen $2p$-metal $3d$ hybridization is reduced in the late-transition-metal oxides.[19] In a first approximation assuming constant O $1s \rightarrow 2p$ matrix elements, the XAS intensity is proportional to the weight of the O $2p$ states in the conduction band. Thus, from the observed intensity ratios in the two spectral regions (see Fig. 5), it is evident that in addition to the Fe $3d$ states, also, the Fe $4sp$ states contribute to the covalent bonding between oxygen and the metal. A usual picture to explain the electronic structure of transition-metal compounds describes the

chemical interaction mainly as a bonding between the metal 4*sp* and 3*d* states, with the ligand *p* states. They form a bonding molecular orbital constituting the occupied valence band and an antibonding combination expanding into the empty conduction band. The symmetry set up by the oxygen ligands determines the type of possible bondings between the central iron and the surrounding ligands. The hybridization is described in terms of the molecular-orbital (MO) language. In the octahedral complex, the metal e_g (d_{z^2}, $d_{x^2-y^2}$) orbitals are directed towards the oxygen ligands and have a strong overlap with the oxygen 2*p* orbitals forming σ bonds. The metal t_{2g} (d_{xy},d_{xz},d_{yz}) orbitals are not directed towards the oxygen ligands, and, therefore, they form π bonds with the oxygen 2*p* orbitals, which are less hybridized than the σ bonds formed by the metal e_g orbitals. The degeneration of the Fe 3*d* energy levels is lifted by the hybridization leading to energetically higher-lying e_g derived bands and lower-lying t_{2g} derived bands. In general, it is assumed that the hybridization of t_{2g} orbitals is about half that of e_g orbitals.[33] The hierarchy of energy levels is reversed in a tetrahedral complex with lower-lying e_g states (forming π bonds) and higher-lying t_{2g} states (forming σ bonds), because the metal t_{2g} orbitals are directed towards the ligand 2*p* orbitals. Furthermore, one has to consider the exchange repulsion between the *d* electrons, which is due to the requirement that the wave function must be antisymmetric, with respect to pairwise permutations of the electron coordinates (Pauli exclusion principle). The exchange effect splits the two groups of bands, t_{2g} and e_g, into four, if it dominates over the ligand-field interaction: spin-up t_{2g}, spin-up e_g, spin-down t_{2g}, and spin-down e_g.

Several theoretical models have been developed to describe the final state accessible in a solid-state environment for electrons excited from an atomic core orbital. For a qualitative interpretation of the features observed within the first electron volts above the threshold, molecular-orbital (MO) theory constitutes a useful tool: it calculates the electronic structure of a cluster consisting of a metal atom surrounded by its oxygen nearest neighbors. In the cubic sodium chloride structure of idealized FeO wustite [see Fig. 6(a)], all Fe^{2+} ions are located on octahedral sites. In the cubic inverse spinel structure of Fe_3O_4 magnetite [see Fig. 1(b)], one-third of the iron ions are located on tetrahedral sites (all Fe^{3+}; filled bonds) and two-third are located on octahedral sites (one-half being Fe^{2+} and the other half Fe^{3+}). In the hexagonal corundum structure of α-Fe_2O_3 hematite all Fe^{3+} ions are located in a slightly distorted octahedral environment [see Fig. 1(c)]. The MO's for Fe^{2+} and Fe^{3+} ions in an octahedral environment have been calculated by Tossell, Vaughan, and Johnson for $[FeO_6]^{10-}$ and $[FeO_6]^{9-}$ clusters representing FeO wustite and α-Fe_2O_3 hematite, respectively.[34] They are shown schematically in Figs. 7(b) and 7(c), respectively. Their MO calculation gives evidence that the O 2*p* and Fe 3*d* orbitals mix to result in the so-called crystal-field split levels t_{2g} and e_g which are separated by the crystal-field splitting energy Δ_0. Furthermore, since the iron oxides exhibit ground states with high-spin values, due to the exchange interaction of the 3*d* electrons, an unrestricted spin calculation was performed.[34] The eigenvalue difference was calculated as being somewhat smaller in the ferrous (Fe^{2+}) case compared with the ferric (Fe^{3+}) case (Δ_0: 1.7 vs 2.2 eV) and the exchange splitting was found to be somewhat larger (*P*: 2.9 vs. 2.7 eV) as shown in Fig. 7. Since spin-pairing requires energy, it is favored if the crystal-field split Δ_0 is larger than the averaged spin-pairing energy *P*, as it is the case for the low-spin complexes. In high-spin complexes, the situation is reversed. It has been found that in the FeO wustite (high-spin complex; octahedral) the highest occupied orbital is the $t_{2g\downarrow}$ containing one electron [see Fig. 7(b)], and in the Fe_2O_3 hematite (high-

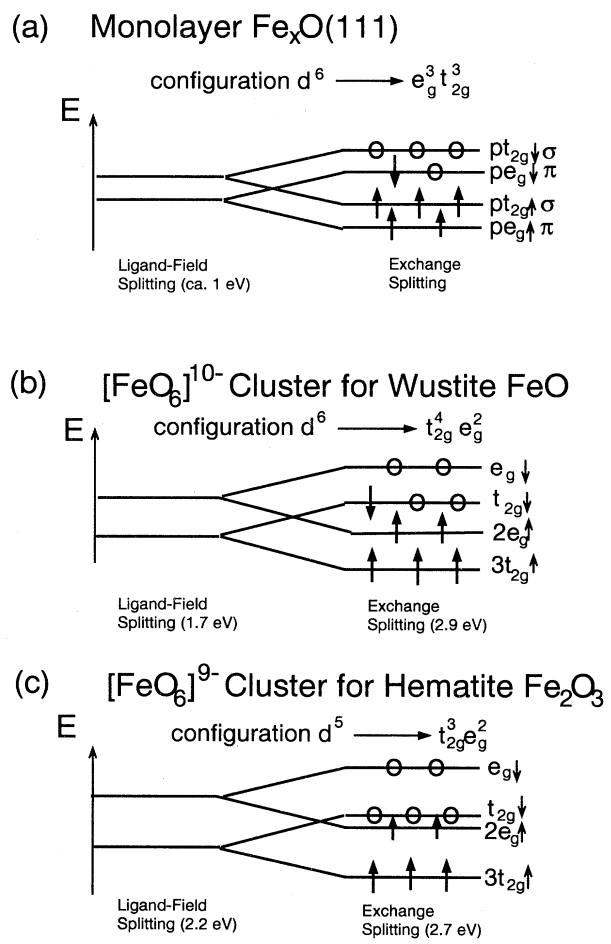

FIG. 7. Molecular-orbital energy diagrams (a) for a trigonal coordinated Fe^{2+} ion in the 1-ML-thick iron oxide film with Fe_xO stoichiometry, (b) for a $[FeO_6]^{10-}$ cluster representing an octahedrally coordinated Fe^{2+} ion in wustite FeO (Ref. 34), and (c) for an $[FeO_6]^{9-}$ cluster representing an octahedrally coordinated Fe^{3+} ion in hematite α-Fe_2O_3 (Ref. 34). The electronic configurations are shown for the hypothetical free ions. In the solid, all the indicated ligand-field and exchange splittings were determined in Ref. 34 by molecular-orbital calculations. The ligand-field splitting of 1 eV for the monolayer was obtained by fitting the experimental data with two Gaussian/Lorentzian curves (see Fig. 8).

spin complex) it is the $2e_{g\uparrow}$ with two electrons [see Fig. 7(c)].

It has been shown, for example, for Ag clusters[38] that the bonding energy of the cluster is weaker and it is more difficult to remove an electron relative to the bulk. Also, the density of states profiles are narrower for the cluster with the Fermi-level energy shifting further from the *d* band towards the vacuum level as the cluster size increases and simultaneously the ionization potential value decreases with cluster size. The cluster approximation is more appropriate for the description of the electronic structure of the monolayer film, because the monolayer can be regarded rather as a two-dimensional bilayer than as a three-dimensional bulk. On the other hand, the Fe_3O_4 and α-Fe_2O_3 multilayer films can be considered as bulk systems, leading to only a qualitative agreement with the cluster MO calculation.

The O *K*-edge spectra of the $Fe_3O_4(111)$ and α-$Fe_2O_3(001)$ multilayers [Figs. 5(b) and 5(c)] exhibit a sharp splitted white line at about 533 eV and a broader structure with two peaks separated by ~ 3.5 eV at about 542 eV. The splitting of the white line distinctly observable at grazing x-ray incidence ($\Theta_e = 20°$) can be identified as the $t_{2g\downarrow}$ and $e_{g\downarrow}$ symmetry bands separated by the ligand-field splitting, as shown in Fig. 7. We fitted the white lines with two combined Gaussian/Lorenzian functions separated by a ligand-field split of 1.3 and 1.5 eV, for the Fe_3O_4 and α-Fe_2O_3 system, which is somewhat smaller than the values from the MO calculations (2.2 eV "crystal-field splitting" for the $[FeO_6]^{9-}$ cluster), but which is in good agreement with recently published data for natural minerals[19] (0.9 eV/1.3 eV for Fe_3O_4/α-Fe_2O_3). Further, the splitting of the two separated peaks agrees with optical data, which reveal a ligand-field splitting of 1.6 eV for the octahedrally hydrated Fe^{3+} ion.[35] These two peaks exhibit a small variation in intensity with Θ_e, and the fit suggests that predominantly the high-energy side peak at 533.6 eV shows a maximum at grazing x-ray incidence ($\Theta_e = 20°$), whereas the first peak remains almost constant in intensity. Although the polarization dependence of the O 1*s* transitions into the unoccupied t_{2g} and e_g orbitals is small for the multilayers due to averaging over many different bond directions considering the probing depth, the polarization dependence of the second peak indicates that it can be assigned to a transition into an unoccupied *pd* orbital with σ symmetry. Considering the MO diagram of the $[FeO_6]^{9-}$ cluster representing the octahedrally coordinated Fe^{3+} ion in hematite α-Fe_2O_3, the ground-state configuration is the high-spin $t_{2g}^3 e_g^2$, with five unpaired electrons. The first peak at 532.3 eV is due to a O 1*s* transition into the $pt_{2g\downarrow}\pi$-orbital and the second peak at 533.8 eV can be attributed to a O 1*s* transition into the $pe_{g\downarrow}\sigma$ orbital. The O *K*-edge spectra of the mixed-valent Fe_3O_4 system show good agreement with the data of the α-$Fe_2O_3(001)$ multilayer, which can be attributed to the fact that the iron oxide is composed of two-third Fe^{3+} ions and only one-third Fe^{2+} ions. Furthermore, Mössbauer spectroscopy studies on the iron oxides have shown that the difference of the electron density of states is very small between the mixed-valent Fe_3O_4 system and the α-Fe_2O_3 system.[37]

It has been suggested in an earlier LEED study on the $Fe_xO(111)$ monolayer that each atom has three nearest neighbors of the other kind: iron atoms are below the center of an oxygen triangle, while oxygen atoms are above the center of an iron triangle leading to a threefold coordination of the Fe^{2+} ions.[6] A starting point for an analysis of the spectra from the $Fe_xO(111)$ monolayer consists in evaluating an MO diagram for an Fe^{2+} ion in a trigonal surrounding, which leads to the same ligand-field splitting as a tetrahedral ligand field, as shown in Fig. 7(a). The iron t_{2g} orbitals are directed towards the oxygen anions in this trigonal array and can mix with the ligand O 2*p* orbitals to form $pd\sigma$ bonds and the iron e_g orbitals can hybridize with the oxygen 2*p* orbitals to form $pd\pi$ bonds. Additionally one has to consider the mixing of Fe 4*sp*- and O 2*p* orbitals resulting in bonding and antibonding σ orbitals. Figure 7(a) shows a qualitative MO-energy diagram for the trigonally coordinated Fe^{2+} ions with the high-spin ground-state configuration of $t_{2g}^3 e_g^3$ and four unpaired electrons. The strong exchange interaction between the six Fe 3*d* electrons, which is larger than the ligand-field splitting, leads to the splitting of the two groups, $pe_g\pi$- and $pt_{2g}\sigma$-orbitals into four states: spin-up $pe_{g\uparrow}\pi$, spin-up $pt_{2g\uparrow}\sigma$, spin-down $pe_{g\downarrow}\pi$, and spin-down $pt_{2g\downarrow}\sigma$. In contrast to the FeO wustite with octahedrally coordinated Fe^{2+} ions, the highest occupied state here is the $pe_{g\downarrow}\pi$ level, containing one spin-down electron. The two other lower-lying occupied states are assigned to the $pt_{2g\uparrow}\sigma$ and $pe_{g\uparrow}\pi$ levels filled with five spin-up electrons. The second higher-lying unoccupied orbital is attributed to the $pt_{2g\downarrow}\sigma$ level separated from the lower-lying $pe_{g\downarrow}\pi$ band by the ligand-field splitting. A transition into these two unoccupied bands is observed in the O *K*-edge spectra of the $Fe_xO(111)$ monolayer in Figs. 5(a) and 8. The first sharp peak at ~ 531 eV is fitted with two combined Gaussian/Lorenzian functions separated by a ligand-field split of 1.0 eV, as shown in Fig. 8. This shows that the origin of the 0.3-eV energy shift between the normal ($\Theta_e = 90°$) and grazing incidence ($\Theta_e = 20°$) spectra can be assigned to a polarization dependence of the O 1*s* transition into these two unoccupied $pe_{g\downarrow}\pi$ and $pt_{2g\downarrow}\sigma$ levels. The π-derived transition exhibits a maximum in intensity at high angles of incidence ($\Theta_e = 20°$), whereas the σ-derived transition shows a maximum in intensity at low of incidence ($\Theta_e = 90°$) (see Fig. 8). We also fitted the broader splitted structure at about 540-eV photon energy with two combined Gaussian/Lorentzian functions separated by 5.0 eV, in order to estimate their polarization dependence as shown in Fig. 8. The absorption edge was represented by an arctan function with the inflection point at the experimentally by XPS determined Fermi-level position of 530.1 eV. These two broader peaks at 537.3 and 542.2 eV, respectively, show a maximum in intensity at normal x-ray incidence ($\Theta_c = 20°$), whereas the σ-derived transition shows a maximum in intensity at low angles of incidence ($\Theta_e = 90°$) and, therefore, they can be assigned to transitions into higher-lying unoccupied states with σ symmetry (O 2*p* character in bonds with predominantly

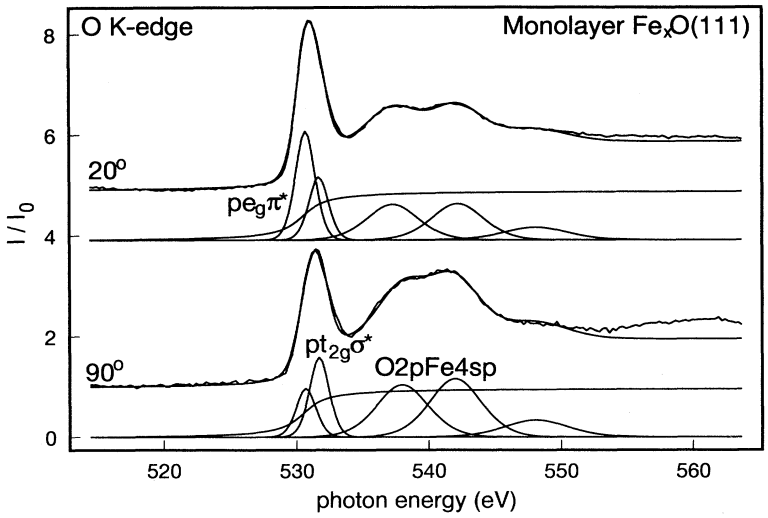

FIG. 8. The O *K*-edge x-ray-absorption spectrum of the ordered monolayer is shown for two angles between the **E** vector of the light and the surface normal **n**, $\Theta_e = 20°$ and 90°. The first sharp peak at ~531 eV is fitted with two combined Gaussian/Lorentzian functions separated by a ligand-field split of 1.0 eV, indicating that the origin of the 0.3-eV energy shift of the white line between the normal and grazing incidence spectrum can be assigned to a polarization dependence of the O 1*s* transitions into the two unoccupied $pe_{g\downarrow}\pi$ and $pt_{2g\downarrow}\sigma$ levels. The broader splitted structure at ~540 eV is also fitted with two combined Gaussian/Lorentzian function separated by 5.0 eV and is attributed to O $1s \rightarrow$ O 2*p* Fe 4*sp* transitions. The absorption edge was represented by an arctan function with the inflection point at the experimentally by XPS determined Fermi-level position of 530.1 eV.

Fe 4*sp* character), in good agreement with Ref. 19.

We assume that the O 1*s* transitions of interest here can be described in a molecular-orbital picture, as dipole transitions into the *p* components of unoccupied $pe_g\pi$ and $pt_{2g}\sigma$ and O 2*p* Fe 4*sp* final states and that their intensities can be derived from Fermi's golden rule as shown for molecules by Stöhr and Outka in Ref. 17. For a 1*s* initial state, the vector matrix element will be directed along the *p*-like final-state orbital and the dipole matrix element assumes the simple form $I = A\cos^2\delta$ [Eq. (1)]; where A describes the angle-integrated cross section and δ is the angle between the electric-field vector **E** and the direction of the final-state orbital, i.e., the direction of maximum orbital amplitude. The equation represents the angular intensity dependence for molecules or bonding units, which can be described by antibonding π and σ *vectors*. The angular dependence of the intensity for molecules with antibonding π and σ *planes* is derived by integrating Eq. (1) over all azimuthal angles in a plane with normal **N**. This yields $I = B\sin^2\varepsilon$ [Eq. (2)], where ε is the angle between **E** and the normal **N** of the plane. The description of the bands within a molecular-orbital model, as suggested for the iron oxides, indicates that the unoccupied $pe_{g\downarrow}\pi$ and $pt_{2g\downarrow}\sigma$ levels can be described by vectors and, furthermore, that the unoccupied O 2*p* Fe 4*sp* bands with σ symmetry can be described by planes. Therefore, the iron-oxygen bond orientation can be determined quite accurately by measuring the transition intensities for only two extreme sample orientations relative to the incident x-ray beam and by comparing the experimental intensity ratio to the predicted theory for the vector- and plane-type orbitals, respectively [for threefold or higher substrate symmetry and a polarization factor of $P = 0.85$ (Ref. 17)]. Our experimentally observed intensity ratios $I(20°)/I(90°)$ of the O $1s \rightarrow pe_{g\downarrow}\pi/pt_{2g\downarrow}\sigma$ transitions are 2.20 (±0.20) and 0.75 (±0.08), respectively. As indicated in Fig. 9, this reveals tilt angles of $\alpha_\pi = 42°$ (±4°) and $\alpha_\sigma = 59°$ (±6°) between the surface normal **n** and the $pe_g\pi$ and $pt_{2g}\sigma$ vector-type orbitals, respectively. Moreover, the experimentally observed intensity ratios $I(20°)/I(90°)$ of the O $1s \rightarrow$ O 2*p* Fe 4*sp* transitions are 0.68 (±0.07) and 0.62 (±0.06), yielding tilt angles of $\varepsilon_1 = 41°$ (±4°) and $\varepsilon_2 = 38°$ (±4°) between the surface normal **n** and the normal of the orbital plane **N** (see Fig. 9). We have detected our O *K*-edge spectra with the **E** vector of the light aligned along the azimuthal direction **a**, which is the direction of the oxygen-oxygen and iron-iron interatomic vectors within a hexagonal close-packed (001) plane (see Fig. 9). The LEED pattern of the monolayer film reveals a (1×1) unit cell with an interatomic distance of 0.320 nm.[5] The four tilt angles that we obtain, α_π and α_σ, ε_1 and ε_2, indicated that the O-Fe-O bond angle projected towards the (**n**,**a**) plane is 104° (±10°) $\{=0.5*[(90°-\alpha_\pi)+\alpha_\sigma+(90°-\varepsilon_1)+(90°-\varepsilon_2)]\}$, as indicated in Fig. 9. Assuming the film to consists of two hexagonal close-packed atomic layers (one oxygen and one iron) with *AB* stacking, the projected angle of 104° (±10°) results in a vertical interlayer spacing of (1.25±0.13) Å and, furthermore, in a corresponding FeO bond length of (2.23±0.22) Å in the monolayer. For comparison, the bond length in bulk is 2.15 Å in FeO.

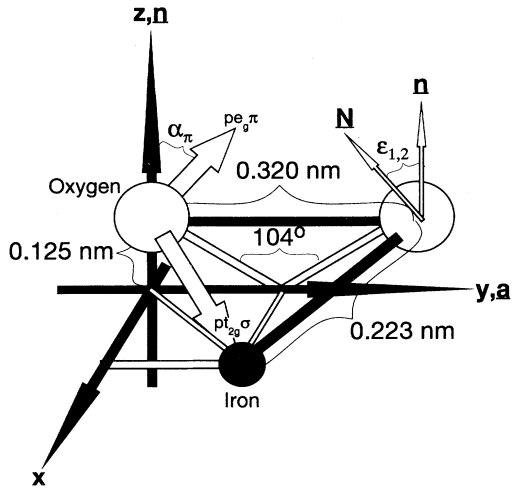

FIG. 9. Schematical picture of an O-Fe-O triangle with oxygen anions aligned along the azimuthal direction **a** and bonded to the iron cation located below the center of an oxygen triangle, as recently suggested in a LEED study on the $Fe_xO(111)$ monolayer (Ref. 6). The LEED pattern of the monolayer film reveals a (1×1) unit cell with an interatomic distance of 0.320 nm (Ref. 5). The two unoccupied $pe_g\pi$- and $pt_{2g}\sigma$-vector-type orbitals have a tilt angle of 42° (±10°) and 59° (±10°), with respect to the surface normal **n** within the (yz) plane. The angles between the normal **N** of the O 2*p* Fe 4*sp*-plane-type orbitals and the surface normal **n**, $\varepsilon_{1/2}=41°$ (±10°)/38° (±10°) are also indicated. The four tilt angles that we obtain indicate that the O-Fe-O bond angle projected towards the (**n**,**a**) plane is 104° (±10°). Assuming the film consists of two hexagonal close-packed atomic layers with *AB* stacking, the projected angle of 104° results in a vertical interlayer spacing of 0.125 nm (±0.013 nm) and, furthermore, in a corresponding FeO bond length of 0.223 nm (±0.022 nm). For comparison, the bond length in bulk is 0.215 nm in FeO.

VII. SUMMARY

The iron oxides form well-ordered epitaxial films, when grown onto Pt(111) surfaces. We prepared a 1-ML film with FeO stoichiometry and 10-ML-thick Fe_3O_4 (magnetite) films. Furthermore, we prepared well-ordered 10-ML-thick α-Fe_2O_3 (hematite) films onto the Pt(111) surface by oxidation of Fe_3O_4 films under high oxygen partial pressures (30 mbar). The films exhibit sharp LEED patterns, which are consistent with the bulk crystal structures of the respective oxides. The 1-ML-thick film consists of an iron-oxygen bilayer that forms a coincidence structure on the platinum substrate. All core-level and valence-band photoemission measurements performed on these films show good agreement with earlier studies on polycrystalline and single crystal samples of iron oxides. They show all features characteristic for the Fe^{2+} and Fe^{3+} species: the corresponding Fe 2*p* and O 1*s* core-level binding energies and satellite structures as well as Fe 3*d* derived final-state valence-band features extending 20 eV below the Fermi level. In the spectra from the monolayer film, we observed additional Fe 3*d* final-state features between the Fermi level and 10 eV below in the valence band when compared to the data performed on cleaved FeO(100) single-crystal surfaces. These additional structures presumably are caused by iron-platinum interactions formed at the substrate-overlayer interface.

The unoccupied conduction-band states were studied by XAS. All spectra agree well with earlier studies on single and polycrystalline iron oxide samples. The O *K*-edge spectra can be understood in terms of the ligand-field theory, considering the exchange interaction between the iron 3*d* electrons. They can be divided into two regions: A white line directly at the threshold and a double-peaked structure 5–20 eV above the threshold. The first one is related to Fe 3*d* states that are hybridized with O 2*p* states and the second one to Fe 4*sp* states that are hybridized with O 2*p* states. In the 10-ML-thick Fe_3O_4 and α-Fe_2O_3 films, the splitting of the white line corresponds to an octahedral oxygen ligand field, while in the monolayer film, this splitting is observed only with the polarization-dependent XAS and is attributed to iron trigonally coordinated by oxygen, which is in line with an iron-oxygen bilayer structure. The observed polarization dependence of the white line in the monolayer spectra indicates that the vertical iron-oxygen interlayer spacing is (1.25±0.13) Å and that the iron-oxygen bond length is (2.23±0.22) Å. This coincides with the corresponding FeO bulk interlayer spacing of 1.24 Å and with the FeO bulk bond length of 2.15 Å. The iron $L_{2,3}$-edge absorption spectrum of the α-Fe_2O_3 films shows a polarization dependence caused by linear magnetic dichroism.

The present characterization forms the basis for the analysis of chemisorption processes and catalytic conversions, such a dehydrogenation reactions. The multilayer films described here can be used in such studies in full equivalence to bulk oxides circumventing all problems mentioned in the introduction. The monolayer film, however, shows some different properties, because it has to be considered as a two-dimensional system that cannot be compared to bulk crystals. It may be viewed as a monolayer of FeO consisting of one iron bilayer, but it cannot be regarded as a monolayer of Fe_3O_4 or α-Fe_2O_3, because more than one bilayer is needed as a repeat unit to build up these structures.

*Author to whom correspondence should be addressed: Th. Schedel-Niedrig, Fritz-Haber-Institut der Max-Planck-Gesellschaft, Faradayweg 4-6, 14195 Berlin (Dahlem), Germany. Electronic address: thomas@carbon.rz-berlin.mpg.de

[1]M. Muhler, R. Schlögl, and G. Ertl, J. Catal. **138**, 413 (1992).
[2]D. Cappus, C. Xu, D. Ehrlich, B. Dillmann, C. A. Ventrice, K. Al Shamery, H. Kuhlenbeck, and H.-J. Freund, Chem. Phys. **177**, 533 (1993); F. Rohr, K. Wirth, J. Libuda, D. Cappus, M. Bäumer, and H.-J. Freund, Surf. Sci. **315**, L977 (1994).
[3]R. J. Lad and J. M. Blakely, Surf. Sci. **79**, 467 (1987).
[4]H. Viefhaus and H. J. Grabke, Surf. Sci. **109**, 1 (1981).
[5]W. Weiss and G. A. Somorjai, J. Vac. Sci. Technol. A **11**, 2138

(1993).
[6]H. C. Galloway, J. J. Benitez, and M. Salmeron, Surf. Sci. **298**, 127 (1993).
[7]W. Weiss, A. Barbieri, M. A. Van Hove, and G. A. Somorjai, Phys. Rev. Lett. **71**, 1848 (1993).
[8]C. R. Brundle, T. J. Chuang, and K. Wandelt, Surf. Sci. **68**, 459 (1977); P. S. Bagus, C. R. Brundle, T. J. Chuang, and K. Wandelt, Phys. Rev. Lett. **39**, 1229 (1977).
[9]A. Fujimori, N. Kimizuka, M. Taniguchi, and S. Suga, Phys. Rev. B **36**, 6691 (1987); A. Fujimori, M. Saeki, N. Kimizuka, M. Taniguchi, and S. Suga, *ibid.*, **34**, 7318 (1986).
[10]R. J. Lad and V. E. Henrich, Phys. Rev. B **39**, 13 478 (1989).
[11]J. Zaanen, G. A. Sawatzky, J. Fink, W. Speier, and J. C. Fuggle, Phys. Rev. B **32**, 4905 (1985).
[12]A. Barbieri, W. Weiss, M. A. Van Hove, and G. A. Somorjai, Surf. Sci. **302**, 259 (1994).
[13]D. E. Eastman and J. L. Freeouf, Phys. Rev. Lett. **34**, 395 (1975).
[14]L. C. Davis, Phys. Rev. B **25**, 2912 (1982).
[15]G. T. Sparrow, B. G. Williams, C. N. Rao, and J. M.Thomas, Chem. Phys. Lett. **108**, 547 (1984).
[16]J. Stöhr and R. Jaeger, Phys. Rev. B **26**, 4111 (1982).
[17]J. Stöhr and D. A. Outka, Phys. Rev. B **36**, 7891 (1987).
[18]A. M. Bradshaw and J. Somers, Phys. Scr. **T31**, 189 (1990).
[19]F. M. F. de Groot, M. Grioni, J. C. Fuggle, J. Ghijsen, G. A. Sawatzky, and H. Petersen, Phys. Rev. B **40**, 5715 (1989).
[20]C. Colliex, T. Manoubi, and C. Ortiz, Phys. Rev. B **44**, 11 402 (1991).
[21]D. W. Fisher, J. Phys. Chem. Solids **32**, 2455 (1971).
[22]L. A. Grunes, R. D. Leapman, C. N. Wilker, R. Hoffmann, and A. B. Kunz, Phys. Rev. B **25**, 7157 (1982).
[23]J. Ghijsen, L. H. Tjeng, J. Van Elp, H. Eskes, J. Westerink, G. A. Sawatzky, and M. T. Czyzyk, Phys. Rev. B **38**, 11 322 (1988).
[24]B. T. Thole and G. van der Laan, Phys. Rev. B **38**, 3158 (1988).
[25]R. D. Leapman and L. A. Grunes, Phys. Rev. Lett. **45**, 397 (1980).
[26]R. D. Leapman, L. A. Grunes, and P. L. Fejes, Phys. Rev. B **26**, 614 (1982).
[27]J. Tafto and O. L. Krivanek, Phys. Rev. Lett. **48**, 560 (1982).
[28]J. H. Paterson and O. L. Krivanek, Ultramicroscopy **32**, 319 (1990).
[29]K. M. Krishnan, Ultramicroscopy **32**, 309 (1990).
[30]C. Colliex, T. Manoubi, and C. Ortiz, Phys. Rev. B **44**, 11 402 (1991).
[31]F. M. M. de Groot, J. C. Fuggle, B. T. Thole, and G. A. Sawatzky, Phys. Rev. B **42**, 5459 (1990).
[32]P. Kuiper, B. G. Searle, P. Rudolf, L. H. Tjeng, and C. T. Chen, Phys. Rev. Lett. **70**, 1549 (1993).
[33]G. A. Sawatzky, in *Narrow Band Phenomena,* edited by J. C. Fuggle, G. A. Sawatzky, and J. W. Allen (Plenum, New York, 1988).
[34]J. A. Tossell, D. J. Vaughan, and K. H. Johnson, Am. Mineral. **59**, 319 (1974).
[35]L. F. Mattheiss, Phys. Rev. **5**, 190 (1972); **5**, 305 (1972).
[36]J. J. Yeh and I. Lindau, At. Data Nucl. Data Tables **32**, 1 (1985).
[37]P. Gütlich, in *Mössbauer Spectroscopy,* edited by U. Gonser, Topics in Applied Physics Vol. 5 (Springer, Berlin, 1975).
[38]R. C. Baetzold, J. Chem. Phys. **68**, 555 (1978).

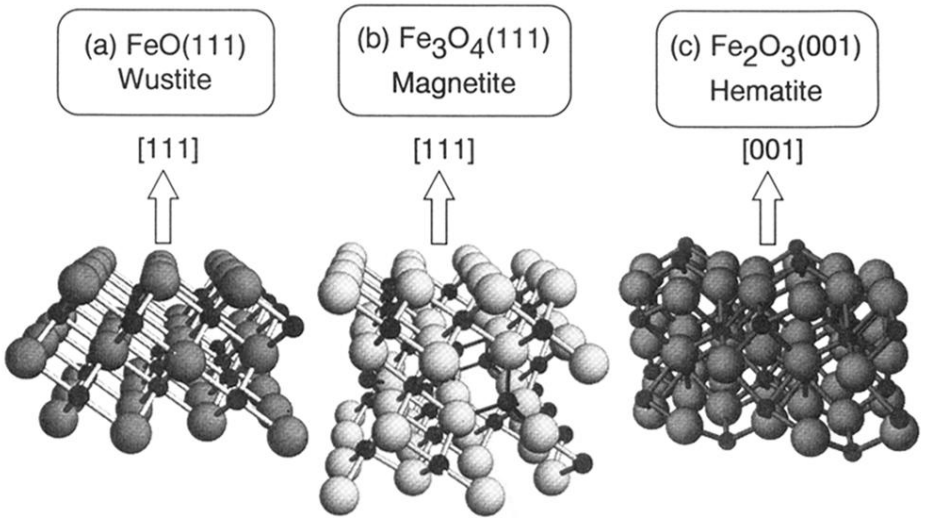

FIG. 1. Perspective side views of ideal bulk terminated iron oxide surfaces: (a) FeO(111) wustite, (b) Fe_3O_4(111) magnetite, and (c) α-Fe_2O_3(001) hematite. FeO (wustite) crystallizes in the cubic sodium chloride structure and contains Fe^{2+} cations (indicated by small filled circles) octahedrally coordinated to the oxygen anions. Fe_3O_4 (magnetite) is ferromagnetic and has a cubic inverse spinel structure with Fe^{2+} cations in octahedral sites and Fe^{3+} cations in both octahedral and tetrahedral sites, the latter indicated by solid bonds. α-Fe_2O_3 (hematite) is antiferromagnetic and has the hexagonal crystal structure of corundum with Fe^{3+} cations located in a slightly distorted oxygen environment.